arXiv:1302.5369v1 [cond-mat.str-el] 21 Feb 2013

Origin of structural transition in $IrTe_2$ studied by single crystal neutron and X-ray diffraction

H. B. Cao,[1, *] B. C. Chakoumakos,[1] J. -Q. Yan,[2, 3] H. D. Zhou,[4, 5] R. Custelcean,[6] and D. Mandrus[2, 3]

[1]*Quantum Condensed Matter Division, Oak Ridge National Laboratory, Oak Ridge, Tennessee 37831, USA*
[2]*Materials Science and Technology Division, Oak Ridge National Laboratory, Oak Ridge, Tennessee 37831, USA*
[3]*Department of Materials Science and Engineering,*
University of Tennessee, Knoxville, Tennessee 37996, USA
[4]*National High Magnetic Field Laboratory, Florida State University, Tallahassee, FL 32306-4005, USA*
[5]*Department of Physics and Astronomy, University of Tennessee, Knoxville, Tennessee 37996-1200, USA*
[6]*Chemical Sciences Division, Oak Ridge National Laboratory, Oak Ridge, Tennessee 37831, USA*

(Dated: February 22, 2013)

We combined single crystal neutron and X-ray diffraction to study the ground state (GS) structure of $IrTe_2$. A structural modulation was observed by both neutrons and X-rays with a wave vector of $\boldsymbol{k}$ =(1/5, 0, 1/5) below T_s≈285 K accompanied by a trigonal to monoclinic lattice distortion. The GS structure lattice was determined to be a_m=6.642(4) Å, b_m=3.965(3) Å, c_m=5.434(3) Å, α_m=90.0(2), β_m=90.0(2), and γ_m=90.1(2) at 5 K. Shortening two of the three nearest Ir-Ir bonds below T_s drives the distortion of the $IrTe_6$ octahedra. The complete GS structure was optimized by matching with the observed X-ray and neutron patterns. Ir 5*d* orbital order is likely the origin of the structural transition.

PACS numbers: 74.62.Fj, 74.25.Dw, 74.70.-b, 74.70.Ad

One of the fundamental issues in the physics of transition metal dichalcogenides (TX_2, T = Ti, Ta, or Nb, X = S, Se, or Te) with 1T and 2H structures is the competition between two very different cooperative electronic phenomena: charge density wave (CDW) state and superconductivity [1–3]. Recently a new member of the TX_2 family incorporating a 5*d* transition metal, $IrTe_2$, has attracted a lot of attention in terms of understanding the relationship between its structural transition and superconductivity when the structural transition is suppressed by doping [4–9]. $IrTe_2$ exhibits a first order structural transition between 250 K and 270 K [10]. At room temperature $IrTe_2$ has trigonal symmetry with edge-sharing $IrTe_6$ octahedra forming layers stacked along the *c*-axis with the Ir ions forming an equilateral triangular lattice in the *ab* plane (Fig. 1(a)). Below the transition temperature, a monoclinic structure was proposed based on powder X-ray diffraction [10]. Accompanied with the structural transition, the resistivity shows a hump-shaped maximum and the magnetic susceptibility drops, which is similar to that of the CDW state in other TX_2 systems. However the early NMR studies did not support the CDW transition scenario in $IrTe_2$ [11]. Recent work found that superconductivity can be induced by suppressing the structural transition by doping small amounts of Pd, Pt, or Cu [4–7]. Pyon *et al.* suggested the structural phase transition is due to Ir 5*d* t_{2g} orbital order or bond order [4, 6]. When the static orbital or bond order is suppressed by doping, the superconductivity appears around the quantum critical point where the orbital or bond order disappears. Photoemission studies [6] suggested the Ir 5*d* orbitals may contribute in the transition. A recent electron diffraction study observed the superlattice peak with a wave vector of (1/5, 0, -1/5), which matches with the Fermi surface nesting wave vector from theoretical calculations [4]. Therefore, orbital-CDW order was suggested as the origin of the structural transition. However recent optical spectroscopy and band structure calculations excluded the CDW origin and suggested the first-order structural phase transition was driven by the crystal field effect mostly from Te 5*p* orbital splitting [8]. The main debate is whether Ir 5*d* t_{2g} orbitals or Te 5*p* orbitals are responsible for the structural transition in $IrTe_2$ and whether the CDW contributes to the transition.

Up to now, all those studies on the structural transition were based on a proposed low temperature structure model from powder X-ray diffraction [10]. Given that electron diffraction observed the existence of superlattice peaks [4], which principally also can be from the structure, the GS structure is probably more complicated than the proposed model. The correct ground state structure of $IrTe_2$ is essential to explore the origin of the structural transition and related electronic properties. In this work, we combined single crystal neutron and X-ray diffraction to measure the GS structure of $IrTe_2$. Two batches of single crystals with different transition temperatures were used in the experiments and both show the modulation vector of (1/5, 0, 1/5), which is different from the electron diffraction measurement [4]. Appearance of the superlattice peaks is due to the distortion of $IrTe_6$ octahedra, which is driven by Ir-Ir bonding. We solved the GS lattice that shows shortening of two of the three nearest Ir-Ir bonds below T_s, which is distinctly different from the widely used structure model [10] where one of the three nearest Ir-Ir bonds was shortened. The complete GS structure was optimized by matching with the observed X-ray and neutron patterns. Ir 5*d* orbital order

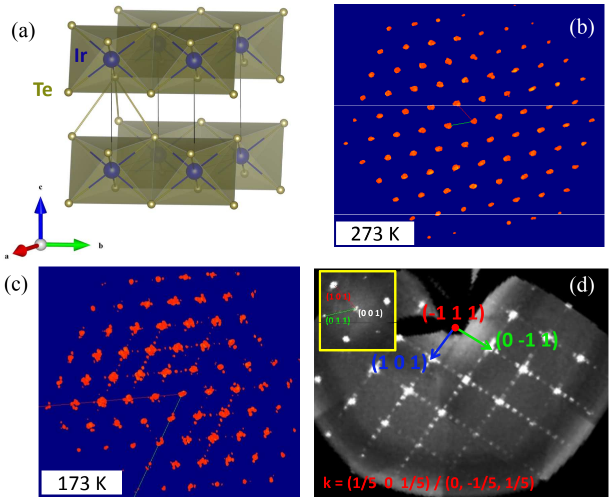

FIG. 1: (Color Online) Sample I: (a) The lattice structure of $IrTe_2$ in the trigonal phase at $T > T_s$ showing the equilateral triangular lattice of Ir atoms in the *ab* plane, brown/blue ball represents Te/Ir. (b) Single crystal X-ray diffraction pattern at 273 K and (c) at 173 K. (d) (H 0 L) reciprocal plane from the pattern in (c) shows the superlattice peaks along the wave vectors of (1/5, 0, 1/5) and (0, -1/5, 1/5). Inset shows (0 0 1) cut from (b), strong (1 0 1) peak and weak (0 1 1) peak are indicated to distinguish (H 0 L) from (0 H L).

is likely the origin of the structural transition.

Single crystals of $IrTe_2$ were grown using self-flux technique as reported [8] but with different cooling rates. Two batches of samples were prepared for the experiments. Sample I has a small crystal size and a lower transition temperature near 264 K and Sample II gives a large enough crystal for neutron diffraction but with a higher structural transition temperature near 285 K. Single-crystal neutron diffraction was performed at the HB-3A four-circle diffractometer at the High Flux Isotope Reactor at Oak Ridge National Laboratory. Neutron wavelengths of 1.542 Å and 1.003 Å were used with a bent perfect Si-220/331 monochromator [12]. Single-crystal x-ray diffraction was performed using a Bruker SMART APEX CCD diffractometer with Mo Kα radiation.

A crystal from Sample I has a structural transition at $T_s \approx 264$K (not shown). Above T_s, a trigonal symmetry $P\bar{3}m1$ pattern was observed (Fig. 1(b)) at T=273 K by X-ray, the lattice parameters are a=3.9298 Å and c=5.3827 Å. Below T_s, at T=173 K, superlatttice peaks appear and the subcell peaks split/broaden (Fig. 1(c)), which makes it difficult to determine the low temperature lattice and to extract the integrated intensities. By making a reciprocal plane cut, the wave vectors of (1/5, 0, 1/5) and (0, -1/5, 1/5) are shown in Fig. 1(d). Since the reflection (1 0 1)/(0 -1 1) and (1 0 -1)/(0 1 1) have the same $\boldsymbol{q}$ length, we only can distinguish them by their

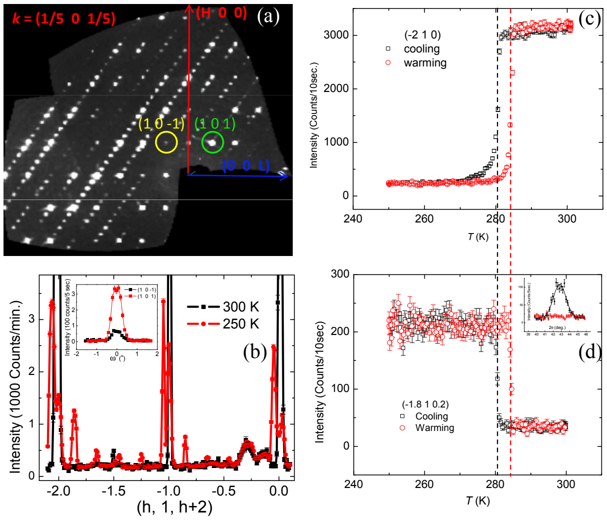

FIG. 2: (Color Online) Sample II: (a) (H 0 L) reciprocal plane from the single-crystal x-ray diffraction at T = 250 K shows the superlattice peaks with a wave vector $\boldsymbol{k}$ =(1/5, 0, 1/5). Subcell peak (1 0 1) and (-1 0 1) are circled in green and yellow to distinguish (H 0 L) from (-H 0 L). (b) $\boldsymbol{q}$-scans along (1 0 1) measured from neutron diffraction at 250 K (black solid square) and 300 K (red solid circle). The scan at 250 K shows the same wave vector of (1/5, 0, 1/5). The strong peak (1 0 1) versus the weak peak (1 0 -1) are also shown in the inset for the same purpose. (c) and (d)Peak intensities of (-2 1 0) and (-1.8 1 0.2) with temperature warming (red open circle) and cooling (black open square) show the first order structure transition accompanied by the superlattice structure modulation. Straight black and red dashed lines are given as guides to the eye. Inset in (d) shows radial scan of (-1.8 1 0.2) at 300 K (red solid circle) and 250 K (black solid square).

intensities, from which we determined the wave vector (1/5, 0, 1/5). The strong (1 0 1) peak is reflected by the dense atomic plane including both Ir and Te atoms, and the relative shifts between the atoms in this plane cause the superlattice periodicity, which differs from (1/5, 0, -1/5) in the structural view. The biggest crystal size from the sample I is about 0.7 × 0.7× 0.05 mm, which is not sufficient for the superlattie peak measurement by neutron diffraction. We selected a crystal with a size of 2.1 × 1.6 × 0.24 mm from the sample II to measure the single crystal neutron diffraction. Its low temperature phase was also checked by single crystal X-rays, and the same wave vector of (1/5, 0, 1/5) was observed (Fig. 2(a)). The structure transition and the modulation vector should not be sample dependent even with different transition temperatures. Single crystal neutron diffraction confirmed that the sample II has the same lattice symmetry but with slightly different lattice parameters of a=3.933 Å and c=5.406 Å at 300 K. Considering the experiment temperature difference, this lattice difference is even smaller. Upon cooling down to 250 K, neutron diffraction also shows the superlattice peaks with the same wave vector of (1/5, 0, 1/5) (Fig. 2(b)). The Figure 2(b) inset shows the reflections of (1 0 1) and (1 0 -1) to confirm that the reciprocal lattice is indexed correctly. The structural transition was tracked by both the subcell peak (-2 1 0) and the superlattice peak (-1.8 1 0.2). The superlattice peaks occur together with the structural transition. Comparing with sample I, a higher transition temperature was found at T_s=285 K during the warming process (Fig. 2(c),(d)). The higher transition temperature may be associated with a faster cooling rate during the sample synthesis. The hysteresis loop with temperature warming and cooling confirms that the structural transition is first-order. Below the transition temperature, the rocking curve scan at (-1 1 1) shows a peak splitting of 3° as compared to a sharp single peak above T_s (Fig. 3(a)). In the measurement at HB-3A, we noticed the rocking curve scan at (-1 1 1) is along (H H 0), which means two domains indicated by the rocking curve scan form. Thus the angle between [-1 1 1] (shown by a red atomic vector in Fig. 3(e)) and [1 1 0] (shown by a blue dashed arrow in Fig. 3(e)) should differ from 90°. Since the reflection (1 1 0) and (0 0 4) retain the single peak upon cooling across the transition, one can generate the lattice parameters by moving Ir1/Ir3 0.067 Å toward Ir2/Ir4 indicated by the black arrows. The proposed atomic shifts involve Ir-Te bonds corresponding to the red and blue atomic vectors in Fig. 3(e). In the same way one can create the other domain by shifting Ir1/Ir3 0.067 Å toward Ir4/Ir2. These two domains yield a peak splitting of 3 ° at (-1 1 1). The lattice parameters obtained in this way are close to the GS lattice obtained at 5 K, a=3.866(3) Å, b=3.965(3) Å, c=5.434(3) Å, α=90.0(2), β=90.0(2), and γ=120.8(2), which is equivalent to another monoclinic lattice of a_m=6.642(4) Å, b_m=3.965(3) Å, c_m=5.434(3) Å, α_m=90.0(2), β_m=90.0(2), and γ_m=90.1(2). The lattice parameters were obtained by refining the motor positions of 40 well centered Bragg peaks. The two equivalent lattices are both shown in Fig. 3(f). The cell volume below T_s is smaller than the one above T_s by 1%, which supports our high pressure studies [9]. Pressure favors the phase with a smaller cell volume and so the structural transition temperature was increased by applying pressure. For convenience, we keep the first lattice definition in the following discussion. In Fig. 3(f), shortened Ir-Ir bonds are indicated by thick blue lines. Ir1-Ir2/Ir3 shortening along a/[1 1 0] can be seen by the 2θ increase of the peak (-2 1 0)/(1 1 0) with temperature decreased (Fig. 3(c)). The (0 0 4) peak in Fig. 3(d) shows the c-lattice increase. Comparing with the early reported monoclinic structure [10], the result is opposite and the current lattice has two Ir-Ir bonds shortening instead of one. However both structure lattices involve shortening of Ir-Ir bonds in certain directions. Due to much better resolution in the 3D reciprocal space, single crystal diffraction can distinguish different reflections coming at the same q length and can fully determine the lattice parameters.

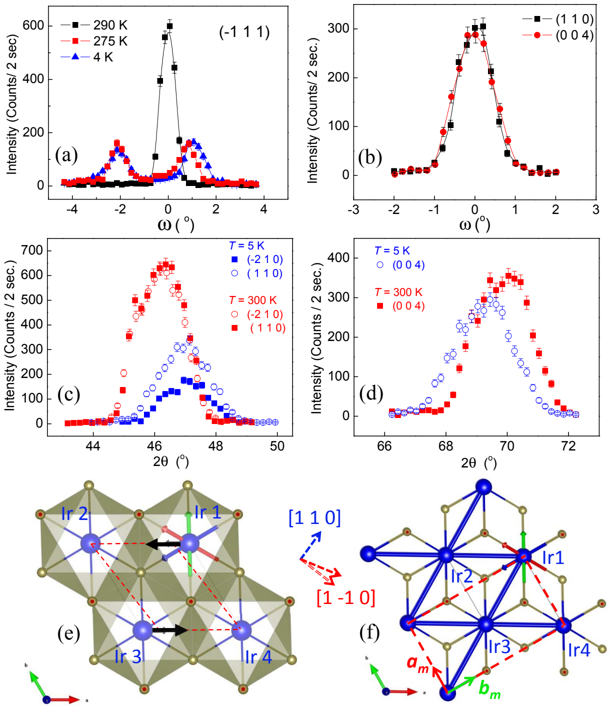

FIG. 3: (Color Online) Sample II: (a) Rocking curve scans of (-1 1 1) at temperatures of 4 K, 275 K, and 290 K show peak splitting across the transition. (b) Rocking curve scans of (1 1 0) and (0 0 4) both show single peak at 250 K . (c) and (d) show the radial scans of (-2 1 0), (1 1 0), and (0 0 4) at 300 K (red) and 5 K (blue). (e) Lattice distortion by shifting Ir1/Ir3 toward Ir2/Ir4 indicated by black solid arrows. Red dashed lines show the distorted lattice. Red/blue/green atomic vector are parallel to [-1 1 1]/[1 0 1]/[0 -1 1] and also correspond to three Ir-Te bond directions. [1 1 0] and [1 -1 0] directions labeled by single dashed arrows are corresponding lattice plane directions after the lattice distortion, and the double dashed arrow represents the other domain with Ir1/Ir3 shifting toward Ir4/Ir2. Two domains make split peaks shown in (a). (f) Distorted lattice corresponding to (e), short Ir-Ir bonds are indicated by thick blue lines. Atomic vectors are the same as the the ones in (e). Red dashed rectangle represents the GS lattice, a_m=6.642(4) Å, b_m=3.965(3) Å, c_m=5.434(3) Å, α_m=90.0(2), β_m=90.0(2), and γ_m=90.1(2). a_m and b_m are labeled. The brown/blue ball represents Te/Ir atom in (e) and (f).

From peak shape and peak intensities, we can conclude the major scattering planes coordinated by Ir atoms remain in the small unit cell of $a \times b \times c$ below T_s except for the lattice distortion mentioned above, while the superlattice peaks are mainly from rearrangement of Te atoms driven by Ir-Ir bonding. For simplicity, we use $P\bar{3}m1$ to do the symmetry analysis, the wave vector of (1/5, 0, 1/5) allows two options of atomic shifting: (1), (0 v 0), shift along b, and (2), v_1=(2u, u, 0), shift in ab plane indicated by black arrows (Fig. 4(a)), and v_2=(0, 0, w), shift along c (see black arrows in Fig. 4(b)). Here u,v, and w represent atomic shift amounts. The second option was found to match with the observed data. By moving Te atoms with two basis vector of (2) adjusted by a phase factor related to the wave vector of (1/5, 0, 1/5), an optimized GS structure model was found. The modeled structure is shown in $5a \times b \times 5c$ lattice in Fig. 4(c). The (1 0 1) lattice planes and the $IrTe_6$ octahedra are plotted to show rearrangement of Te atoms. The calculated X-ray pattern (Fig. 4(d)) generally matches with observed one (Fig. 2(a)).

Ir-Ir bond shortening suggested Ir-Ir bonding through Ir^{4+} $5d$ orbital overlap. We can apply a similar theory described in the early paper by Pyon *et al.* [4, 6] to the current GS structure. We define local coordinations at Ir sites, x, y, z are represented by the atomic vectors in red, green, and blue color, respectively (Fig. 3(e-f) and Fig. 4(a-b)). Above T_s, due to the trigonal symmetry, 5 $5d$ electrons of Ir^{4+} distribute at 3 degenerate low energy level t_{2g} orbitals, d_{xy}, d_{yz}, and d_{zx}. Below T_s, Ir-Ir bonding along yz and zx removes partial orbital degeneracy and 3 orbitals have d_{xy} at lower energy level, d_{yz} and d_{zx} in higher energy level. The d_{xy} orbital is fully filled and repels two nearest Te atoms away, indicated by black arrows (Fig. 4(a-b)). While at the bonded Ir-Ir, d_{yz} and d_{zx} have a hole, which attracts two nearest Te atoms along z (Fig. 4(a-b)). The attracted Ir-Te bonds along z also can result in the reported Te $5p$ orbital spliting with p_z higher than p_x and p_y [8]. Due to lattice contraction in the ab plane caused by Ir-Ir bonding, the Te atom shifts mainly along c, two of six nearest Te atoms around each Ir site are attracted, i.e., most of Te atoms are repelled, which causes c-lattice increase. In the GS structure, the volume of the $IrTe_6$ octahedra are also modulated, which may imply CDW existence. Since the cell volume change is higher than 1% across the transition, the high symmetry structure with the biger cell volume above T_s is extremly unstable and is highly sensitive to pertubation. Therefore, orbital order with low energy scale can relieve the structure instability and completely reconstruct the structure.

In conclusion, we measured the GS structure of $IrTe_2$ by single crystal neutron and X-ray diffraction. The superlattice peaks were observed in both measurements with the same wave vector of (1/5, 0, 1/5). The GS structure lattice revealed two of the three nearest Ir-Ir bonds are shortened and one is elongated, which is due to Ir-Ir bonding through Ir^{4+} $5d$ t_{2g} orbital overlap. Ir^{4+} $5d$ orbital order results in Te atoms shifts and reduce the cell volume by 1%, i.e., releaving the geometrical frustration of the instable high-temperature structure. The superlattice peaks are mainly contributed by Te atoms. The modeled GS structure shows varient volume of $IrTe_6$ octahedra, which implies possible exisistence of CDW state. Ir^{4+} $5d$ orbital order as a pertubation is the origin of the structural transition in $IrTe_2$.

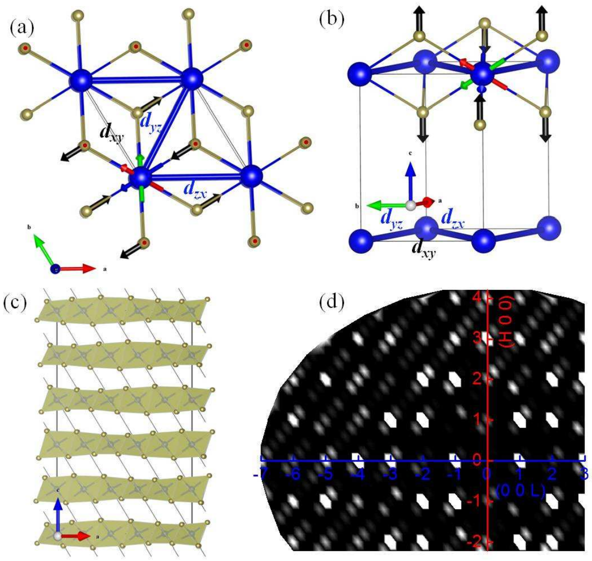

FIG. 4: (Color Online) (a) and (b) The lattice structure of $IrTe_2$, the brown/blue ball represents Te/Ir atom. Shifts of Te atoms along [2 1 0] and [0 0 1] are denoted in black arrows. Local coordinations at Ir sites x, y, and z are indicated by the atomic vector in red, green, and blue color, respectively. Three Ir $5d$ t_{2g} orbitals, d_{xy}, d_{yz}, d_{zx} can be recognized by the local site coordinations. (c) Optimized GS structure with $5a \times b \times 5c$ lattice. $IrTe_6$ octahedra and (1 0 1) lattice planes are plotted. (d) (H 0 L) reciprocal plane of the calculated X-ray pattern from the structure in (c).

This work was supported by the US Department of Energy, Office of Basic Energy Sciences. HBC and BBC are supported by the Scientific User Facilities Division, JQY and DGM are supported by the Materials Science and Engineering Division, RC is supported by the Division of Chemical Sciences, Geosciences, and Biosciences.

---

[*] Electronic address: caoh@ornl.gov

[1] R. L. Withers and J. A. Wilson, J. Phys. C **19**, 4809 (1986).
[2] J. A. Wilson and A. D. Yoffe, Adv. Phys. **28**, 193 (1969).
[3] J. A. Wilson, F. J. DiSalvo, and S. Mahajan, Adv. Phys. **24**, 117 (1975).
[4] J. J. Yang, Y. J. Choi, Y. S. Oh, A. Hogan, Y. Horibe, K. Kim, B. I. Min, S-W. Cheong, Phys. Rev. Lett. **108**, 116402 (2012).
[5] S. Pyon, K. Kudo, and M. Nohara, J. Phys. Soc. Jpn. **81**, 053701 (2012).
[6] D. Ootsuki, Y. Wakisaka, S. Pyon, K. Kudo, M. Nohara, M. Arita, H. Anzai, H. Namatame, M. Taniguchi, N. L. Saini, and T. Mizokawa, Phys. Rev. B **86**, 014519 (2012).

[7] M. Kamitani, M. S. Bahramy, R. Arita, S. Seki, T. Arima, Y. Tokura, and S. Ishiwata, arXiv:1212.6116 (2012).

[8] A. F. Fang, G. Xu, T. Dong, P. Zheng, and N. L. Wang, Nature Sci. Rep. **2**, 1153 (2013).

[9] A. Kiswandhi, J. S. Brooks, H. B. Cao, J. Q. Yan, D. Mandrus, Z. Jiang, H. D. Zhou, arXiv:1212.5330 (2013)

[10] N. Matsumoto, K. Taniguchi, R. Endoh, H. Takano, and S. Nagata, J. Low. Tem. Phys. **117**, 1129 (1999).

[11] K. Mizuno, K. Magishi, Y. Shinonome, T. Saito, K. Koyama, N. Matsumoto, and S. Nagata, Physica B **312-313**, 818 (2002).

[12] B. C. Chakoumakos, H. Cao, F. Ye, A. D. Stoica, M. Popovici, M. Sundaram, W. Zhou, J. S. Hicks, G. W. Lynn, and R. A. Riedel, J. Applied Cryst., **44**, 655 (2011).